Ducted wind turbines in yawed flow: A numerical study

Vinit Dighe[1], Dhruv Suri[2], Francesco Avallone[1], and Gerard van Bussel[1]

[1]Wind Energy Research Group, Faculty of Aerospace Engineering, Technological University of Delft, Netherlands
[2]Renewable Energy Research Group, Department of Aeronautical and Automobile Engineering, Manipal Institute of Technology, India

Correspondence: Vinit Dighe (v.v.dighe@tudelft.nl)

Abstract. Ducted Wind Turbines (DWTs) can be used for energy harvesting in urban areas where non-uniform flows are caused by the presence of buildings or other surface discontinuities. For this reason, the aerodynamic performance of DWTs in yawed flow conditions must be characterized. A numerical study to investigate the characteristics of flow around two DWT configurations using a simplified duct-actuator disc (AD) model is carried out. The analysis shows that the aerodynamic performance of a DWT in yawed flow is dependent on the mutual interactions between the duct and the AD; an interaction that changes with duct geometry, AD loading and operating conditions. It is found that the duct cross-section camber returns a gain in performance up to a specific yaw angle; thereafter any further increase of yaw angle results in a performance drop.

1 Introduction

Global energy demand is expected to more than double by 2050 owing to the growth in population and economy (Gielen et al., 2019). The global wind power capacity quadrupled in less than a decade reaching 597 Gigawatt by the end of 2018 compared to 120 Gigawatt in 2008 (Dupont et al., 2018). Wind turbines are typically installed away from populated areas considering the enforced visual and noise regulations. This necessitates the transfer of electricity via grids over large distances, which increases the levelized cost of electricity (LCOE). However, the integration of wind turbines into urban areas is challenging; the presence of buildings, trees and surface discontinuities lead to lower wind speed, non-uniform inflow and larger turbulent fluctuations compared to open fields. To address these challenges, design modifications of wind turbines, suitable for operation in an urban setting is required.

A possible technological solution to extract wind energy in urban areas is represented by Ducted Wind Turbines (DWTs). DWTs increase energy extraction with respect to conventional horizontal axis wind turbines (HAWTs) for a given turbine radius and free-stream velocity (van Bussel, 2007). DWTs are constituted of a turbine and a duct (also named as diffuser or shroud); the role of the latter is to increase the flow rate through the turbine relative to a similar turbine operating in the open atmosphere, thus increasing the generated power. This is more than one explanation for how this occurs. The first explanation is that the duct forces an expansion of flow downstream of the turbine beyond what is attainable for a bare wind turbine. This provides a reduced pressure behind the turbine, and increase the total mass flow through the turbine (van Bussel, 2007). A second explanation (de Vries, 1979), different in nature but conceptually similar, is that if the sectional lift force of the duct is directed towards the turbine plane, then the associated circulation (see Figure 1) of the duct increases the mass flow through

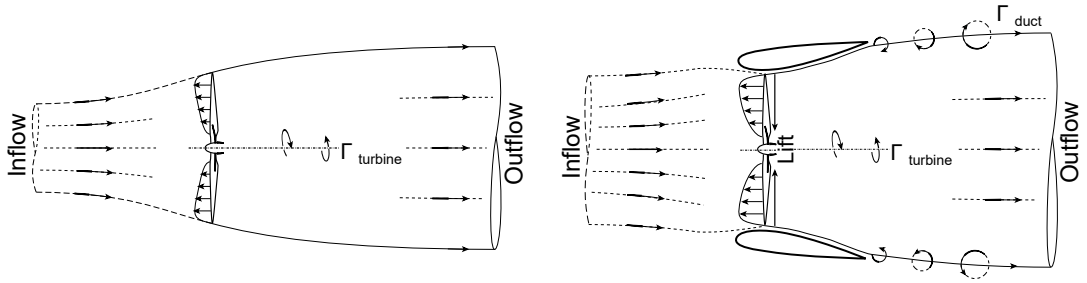

Figure 1. Schematic of stream-tube model for a bare turbine (left) and DWT (right). The bound circulation from the turbine blades and the duct surface is denoted by τ

the turbine. A significant amount of literature on DWTs, based on the combined use of theoretical, numerical and experimental techniques, exists (Igra, 1981; Gilbert and Foreman, 1983; Abe et al., 2005; Toshimitsu et al., 2008; Werle and Presz, 2008; Khamlaj and Rumpfkeil, 2017). Questions over the performance of DWTs in yawed flow remain, however.

Igra (1981) studied experimentally the effects of yaw on the performance of DWTs. Eight geometries were investigated using different duct profiles and an actuator disc (AD) model to represent the turbine. The eight configurations differed in the duct expansion ratio, i.e., the ratio of exit area of the duct to the turbine area. The AD has a thrust coefficient of approximately 0.5. It was found that when the duct expansion ratio was less than 4.5, little or no difference in the power output was measured up to a yaw angle of $\pm$ 30° while any further increase in yaw resulted in power reduction. On the other hand, when the duct expansion ratio was higher than 4.5, the generated power decreased even for small yaw angles. Igra explained that the yaw insensitivity, for the low duct expansion ratio configurations, is due to the lift force increase by the annular duct section. The author did not provide any further explanation to further clarify the physics behind performance drop for large duct expansion ratio. On the same line, researchers from Grumman Aerospace tested a bare turbine and two DWT models (named as Baseline DAWT and DAWT 45) varying the yaw angle up to 40° with increments of 10° (Gilbert and Foreman, 1983). Both the Baseline DAWT and DAWT 45 models showed a negligible change in the power up to a yaw angle of 30°, and a drastic reduction in power at yaw angle of 40°. Surprisingly, the bare turbine also demonstrated no dependence on the yaw angle up to 30°. They stated that this was due to the long center-body configuration, similar in all the three designs, that helped channeling the incoming flow towards the upwind turbine blade and at the same time shielding the downwind turbine blade, thus offering an insensitivity to yaw. However, in a follow up paper (Foreman and Gilbert, 1983) they stated that these yaw tests were inconclusive whether the yaw insensitivity was due to the center-body effect or the duct geometry itself. More recently, Phillips et al. (2002) combined experimental and numerical analysis to study DWTs under yawed flow. They concluded that the power increase for a DWT in yawed flow can only be achieved with a slotted duct design (named as Mo), with the added mass flow of air through the slot increasing the boundary layer flow control and preventing flow separation over the suction side (inner surface) of the duct under severe yaw misalignment.

The above literature, due to the contrasting nature of the conclusions, lacks clarity on the aerodynamics of DWTs in yawed flow, and particularly on the effect of the duct geometry on the aerodynamic performances. The goal of this paper is to focus

on the latter; this is performed using Unsteady Reynolds Averaged Navier Stokes (URANS) CFD approach. To this aim, two reference duct geometries are selected and the turbine is simulated by a uniformly loaded AD model (Dighe et al., 2019a, b). The numerical AD model has been been applied by Mikkelsen and Sørensen (2001) to study the flow on a horizontal axis wind turbine in axial and yawed inflow conditions. The numerical predictions agree reasonably well, both in axial and yawed inflow conditions, when compared to the measurements on the Tjæreborg 2MW field turbine. This model is also employed by Tongchitpakdee et al. (2005) to study yaw; the NASA-Ames experiments of the NREL Phase VI turbine are modeled for yaw angles from 0° to 45° to find reasonable agreement with the experiments. The numerical AD model has the potential to implicitly model an unsteady, asymmetric wake, and thus capture the first order flow physics; for higher order effects, the blades have to be resolved (Haans, 2003).

The paper is organized as follows. Section 2 reports the non-dimensional coefficients adopted for characterizing the aerodynamic performance of the duct-AD model, both under non-yawed and yawed flow conditions. Section 3 describes the numerical settings and parameters with the description of the duct profiles chosen for the current investigation. Section 4 reports the numerical validation study. Insights on the aerodynamic performance coefficients with respect to yawed flow will be discussed in section 5, together with flow analysis. Finally, the most relevant results are summarized in the conclusions.

2 Duct - AD flow model

The turbine is modelled by a flat AD of infinitesimal width. The AD exerts a constant thrust force T_{AD}, calculated across the AD surface S_{AD}, which corresponds to a non-dimensional thrust force coefficient:

$$C_{T,AD} = \frac{T_{AD}}{\frac{1}{2}\rho {U_\infty}^2 S_{AD}}, \tag{1}$$

where ρ is the fluid density and U_∞ is the free-stream velocity.

To generate T_{AD}, a uniform pressure drop is present across the AD surface, $T_{AD} = \Delta p \times S_{AD}$. The pressure drop Δp is taken from experiments (Tang et al., 2016) and is given as an input parameter to the numerical simulations. The mean velocity across the AD radial plane, which is a function of AD thrust coefficient $U_{AD_0} = f(C_{T,AD})$, can be expressed by integrating the difference of the free-stream velocity component U_x across the AD surface:

$$\frac{U_{AD_0}}{U_\infty} = \frac{1}{S_{AD}} \oint_{S_{AD}} U_x dS. \tag{2}$$

Using Eqs. 1 and 2, the power coefficient for a bare AD reads:

$$C_{P_o} = \frac{U_{AD_0}}{U_\infty} C_{T,AD}. \tag{3}$$

The subscript 0 has been adopted for quantities evaluated for bare AD configuration.

For a duct-AD configuration, an additional thrust force exerted by the duct on the flow, or vice-versa, appears. Then, the total thrust force T is the vectorial sum of the AD thrust force T_{AD}, and the duct thrust force T_D, given by:

$$T = T_{AD} + T_D. \tag{4}$$

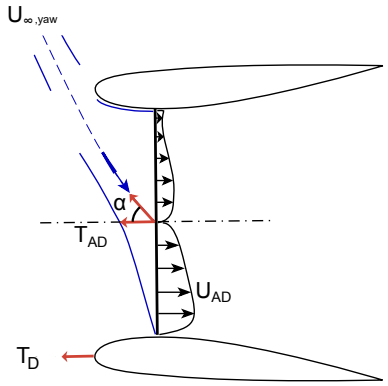

Figure 2. Schematic of yawed flow around a duct-AD model

The total thrust coefficient is then defined as:

$$C_T = C_{T,AD} + C_{T,D}. \tag{5}$$

Note that the duct thrust coefficient $C_{T,D}$ is normalized with the AD area S_{AD} to facilitate direct addition to the AD thrust coefficient $C_{T,AD}$ for calculating the total thrust coefficient C_T. Then, the mean velocity at the AD for a duct-AD model is a bivariate function of AD thrust coefficient and the duct thrust coefficient: $U_{AD} = f(C_{T,AD} + C_{T,D}) = f(C_T)$. Similar to Eq. 3, the power coefficient for the duct-AD model, using S_{AD} as the reference area, becomes:

$$C_P = \frac{U_{AD}}{U_\infty} C_T. \tag{6}$$

The power coefficient expression in Eq. 6 challenges the well-known Lanchester–Betz–Joukowsky limit of $\frac{16}{27}$ for maximum power coefficient obtainable for a HAWT. This should not appear like a surprising result, since, the mass flow of air swallowed in the presence of a duct is greater due to the additional thrust force $C_{T,D}$ offered by the duct. The above relations are also valid for the DWT under yawed flow condition. Figure 2 shows the schematic of flow around the duct-AD model, where α is the yaw angle relative to the incident free-stream direction.

3 Methodology and Computational Setup

A commercial CFD solver ANSYS Fluent® has been used for a complete viscous transient solution of incompressible flow around the duct-AD model. The governing flow equations are URANS equations. A detailed description of the the governing equations is beyond the scope of the current discussion; the reader may refer to Versteeg and Malalasekera (2007).

The 2D and 3D computational domain is shown in Figure 3, where the distance from the AD location to the domain inlet and outlet are $12c$ and $24c$, respectively. For the present computations, a C-grid structured zonal approach is chosen, see Figure 3, which proved advantageous in the case of a curved boundary, i.e. duct's leading edge. The C-shaped loop terminates in the

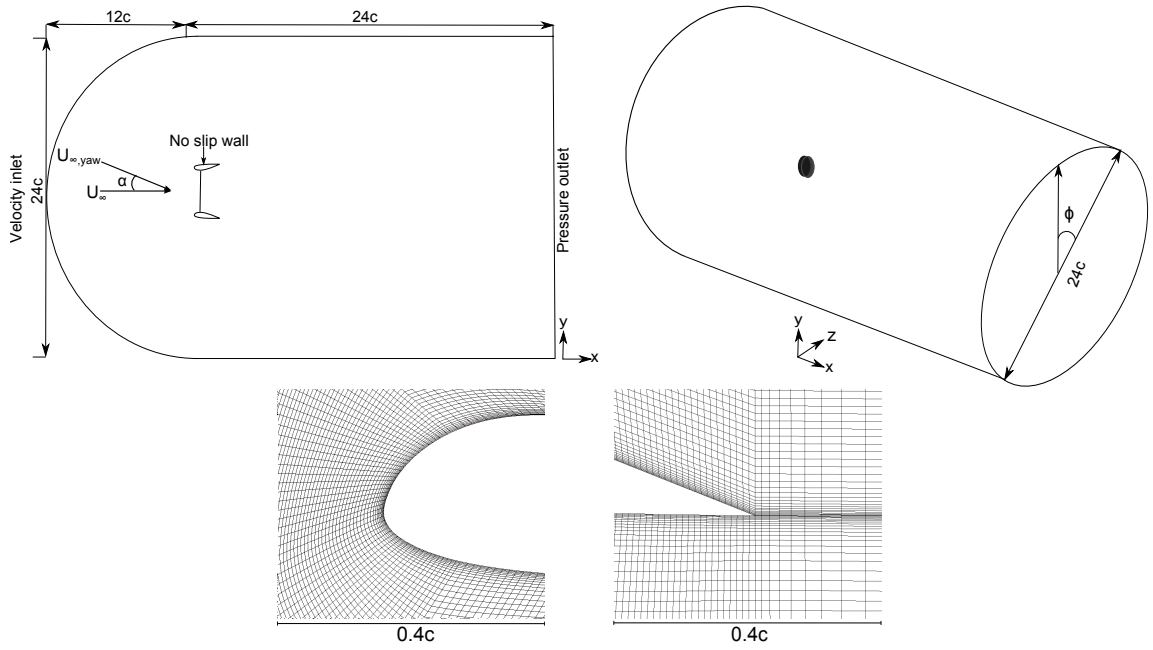

Figure 3. Computational domain showing the boundary conditions employed (top). The lengths are normalized with the duct chord length c. Representative, not to scale. Computational grid surrounding the leading and trailing edge of the duct (bottom).

wake region. The computational grid consists of quadrilateral cells with maximum y^+ value of ≈ 1 on the duct wall (see Figure 4). Then, through extruding the grid using 100 grid points in azimuthal direction ϕ, 3D structured grid is generated.

Boundary conditions are: uniform velocity at the inlet, zero gauge static pressure at the outlet, no-slip walls for duct surfaces. The influence of AD is included into the domain as an additional body force acting opposite to the direction of flow. This is achieved using a reverse fan boundary condition in ANSYS Fluent®. For a uniform thrust loading, the thrust force is given by:

$$T_{AD} = \frac{C_{T,AD}\rho U_\infty^2}{2}, \tag{7}$$

where $C_{T\,AD}$ is calculated from a semi-empirical relation of pressure drop curve and the velocity at the AD obtained from wind tunnel experiments. The fluid is air with fluid density ρ = 1.276$\frac{kg}{m^3}$ and dynamic viscosity $\mu = 1.722 \times 10^{-5}\ Pa{\cdot}s$. Values of free-stream velocity U_∞ and turbulence intensity I are chosen for consistency with the wind tunnel experiments. To establish yawed inflow conditions, the flow is rotated around the center-line axis by yaw angle α for different test cases.

k-ω SST (shear stress transport) model is used as turbulence model. Preliminary investigations showed good agreement with the experiments (Dighe et al., 2019a, b). The URANS solutions are obtained using the SIMPLE algorithm based on the recommendations of Fluent (2011). A least-squares cell-based method is used to evaluate the pressure gradient, with continuity and momentum equations solved using a second order upwind differential scheme. The convergence criteria is set to 10^{-6} for

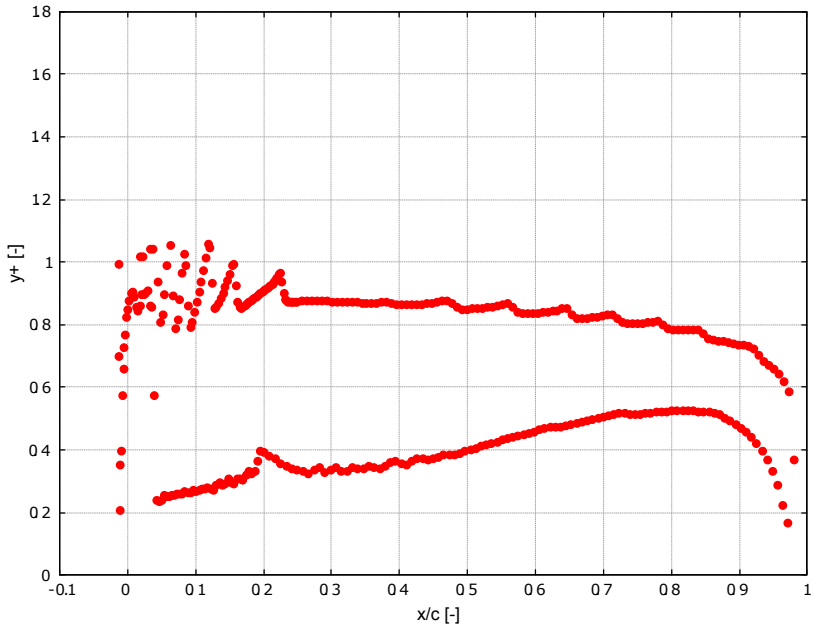

Figure 4. Dimensionless y+ distribution on the duct wall surface.

all the residuals. The simulations are run corresponding to a physical time of 6 seconds, or 40 complete rotations of the turbine blades. The physical time step Δt, corresponding to a Courant–Friedrichs–Lewy (CFL) number of 1 in the finest mesh refined regions is 2.67×10^{-4} s. A typical converged 2D URANS solution with approximately 0.1 million mesh elements is obtained in roughly 30 minutes on a quad-core work-station desktop computer. The converged 3D URANS solution with approximately 10 million mesh elements is obtained in roughly 54 hours on a quad-core work-station desktop computer.

4 Numerical validation

For validating the numerical approach, experiments carried out by Igra (1981) on a different duct-AD geometry are simulated. Igra's experiments were conducted in the subsonic wind tunnel of the Israel Aerospace Industry (formerly Israel Aircraft Industry); this tunnel has a large test section and it measures 3.6 m $\times$ 2.6 m.

A schematic of the cross-section geometry (named as Model B) is shown in Figure 5(a). The longitudinal cross-section of the duct is a NACA 4412 airfoil. The leading edge of the duct is rotated by 2° with respect to the free-stream direction, resulting in a duct expansion ratio $\frac{S_e}{S_{AD}}$ = 1.54. A uniformly loaded AD model with $C_{T,AD}$ = 0.434 is used to represent the turbine. The experimental data set consists of: static pressure distribution at different axial and radial positions, and forces generated by the duct surface for a range of flow angles. During the experiments, the inflow velocity was set at U_∞ = 32 m/s. Following Igra (1981), the wall interference and blockage correction can be ignored. The experimental data is reported in terms of the

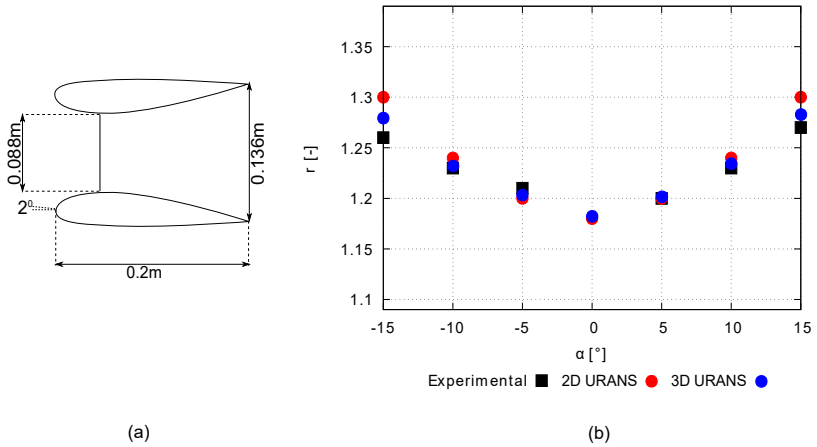

Figure 5. A schematic cross-section layout of the three dimensional experimental model used for the numerical validation study (a), and comparison between experimental findings (Igra, 1981) and the CFD results (b).

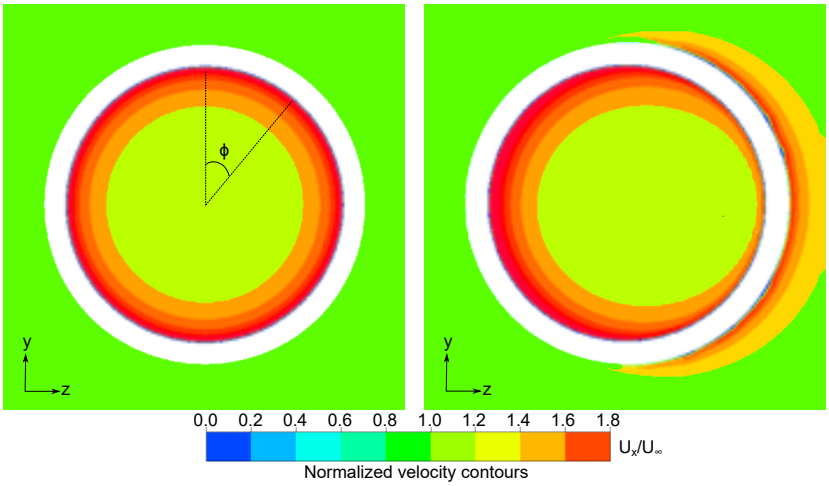

Figure 6. Contours of time-averaged non-dimensional free-stream velocity U_x/U_∞ measured at the AD location located in the $y-z$ plane for Model B in (left) non-yawed inflow and (right) yawed inflow, α = 10°.

augmentation factor $r = \frac{C_P}{C_{P_o}}$, which expresses the ratio between the power coefficient of the duct-AD model and the power coefficient of the bare AD model when both the models bear the same AD and similar operating conditions.

A good agreement between the CFD simulations and the experimental findings is found in Figure 5(b). The deviation between the CFD and the experimental findings increase with increasing values of α, especially for 2D URANS calculations.The differences in the 2D and 3D CFD results can be explained by looking at the flow field obtained using 3D URANS simulations. Figure 6 shows the time-averaged velocity contours of non-dimensional axial velocity $\frac{U_x}{U_\infty}$ in the $y-z$ plane at the AD location for Model B in non-yawed (left) and yawed (right) inflow conditions. Time averaging is performed after convergence

Table 1. Grid statistics for grid independence study of the reference case.

Grid	Number of cells	$C_{T,D}$
Coarse	67640	0.3012
Medium	102008	0.3133
Fine	161028	0.3135

is reached. Because of the yaw angle (α = 10°), an asymmetric flow field is present, thus the velocity at the AD plane changes with the azimuthal angle Φ. Here, the azimuthal angle Φ is defined as positive in the clockwise direction when looking from upwind, with zero when oriented in the positive y direction, see Figure 6 (left). The main difference between the two results is due to fact that the C_P (equation 6) obtained from 3D URANS simulations uses the azimuthally averaged streamwise velocity component, while the results from 2D simulations do not account for the gradual variation with Φ. However, as shown in the comparsion, the three dimensional azimuthal effects are negligible when comparing r. It is important to highlight that the maximum deviation between 2D URANS results and experimental findings is less than 5% for α = 15°.

For an additional validation of the AD approach, numerical results obtained using 2D and 3D URANS are compared with the experimental study reported by Ten Hoopen (2009). The study was conducted using the full scale DonQi® DWT model in non-yawed inflow condition (see Figure 7). Experiments were conducted in the closed-loop open-jet (OJF) wind tunnel facility at the Delft University of Technology. The average thrust coefficient of the turbine $C_{T,turbine}$ was measured in the experimental study to be 0.689; this value is chosen to model $C_{T,AD}$ for the results presented. Figure 7 shows the comparison of the normalized free-stream velocity $\frac{U_x}{U_\infty}$ measured behind the turbine blade at $x/c = 0.37$ in the radial direction y. Transition was not forced but the experimental model has a noise damper, see Figure 7, which acts as rough surface that forces transition to turbulence; this has not been replicated numerically. The computed velocity profiles preserves the overall shape, with the relative difference, calculated lower than 10%, which is within the experimental uncertainty and also attributed to the absence of discrete blades and their related effects such as tip vortices, wake rotation and an accelerated mixing of the flow through the DWT with the external flow.

The 2D URANS approach gives results of reasonable accuracy when compared to the 3D URANS approach. The computing cost issued by going from 2D URANS to 3D URANS does not justify the scope of the current study, where the effects of distributed AD loading, wake rotation and divergence are totally ignored. Having said that, the 2D URANS approach combined with numerical duct-AD model has been adopted for the results presented, hereinafter.

A grid independence analysis has been carried out for the 2D grid using three grid sizes, where the refinement factor in each direction is 1.5. Refinement factor is defined as the rate at which the grid size increases in the direction normal to the surface of the wall (duct surface). The duct thrust force coefficient $C_{T,D}$ is taken as reference for the convergence analysis. The results of the grid independence study are shown in Table 1. Convergence is reached for the medium refined grid, where the $C_{T,D}$ value fluctuates less than 0.0003%, and similar grid refinement is used in the numerical investigation, hereinafter.

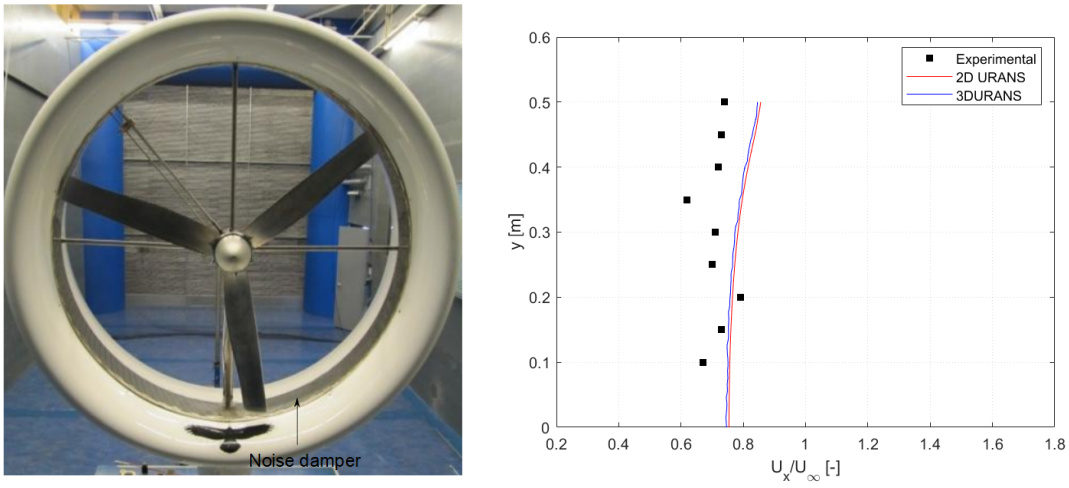

Figure 7. Comparison of dimensionless velocity profile vs radius from centerline between the experimental data and the CFD findings shown for DonQi®DWT model in non-yawed inflow condition.

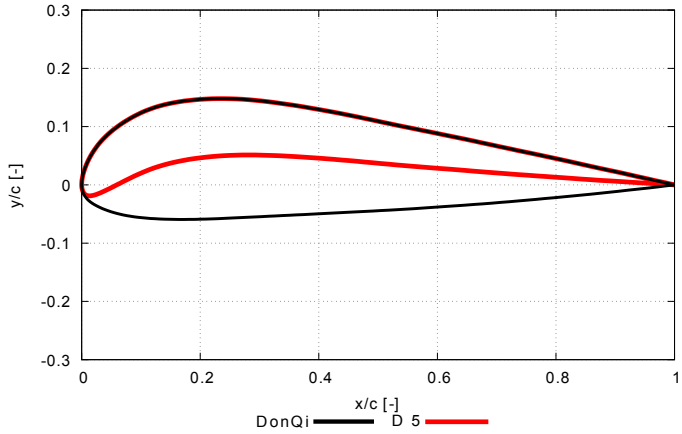

Figure 8. Cross-sectional geometry of the lower duct used for the numerical study.

5 Results and Discussion

5.1 Duct geometries

Two duct geometries, shown in Figure 8, with different longitudinal cross section (named as DonQi® and DonQi D5) are chosen for the current investigation. The selection is based on the duct shape parametrization study conducted by the authors (Dighe et al., 2019b). The parametrization procedure for duct shapes preserved the following geometric features: leading edge position (which defines the inlet area ratio), trailing edge position (which defines the exit area ratio) and inner side thickness (which preserves AD radius and clearance). This makes it ideal to isolate the effects of the duct cross-section on the aerodynamic

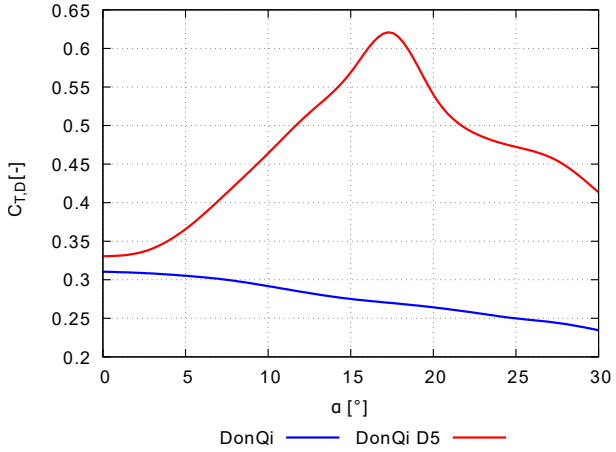

Figure 9. Effect of yawed inflow on the duct thrust force coefficient for the two duct geometries. $C_{T,AD} = 0.7$.

performance of the duct-AD model in yaw. In the study, an optimal $C_{T,AD} = 0.7$ was obtained for both the duct geometries. This value is employed for the rest of the discussion.

5.2 Duct force coefficient

Figure 9 illustrates the variation of duct force coefficient $C_{T,D}$ as a function of yaw angle α obtained for the two duct geometries investigated in this study. $C_{T,D}$ trend-lines are obtained using the results from thirteen simulations ranging from α = 0°-30° with increment of 2.5°. Starting with the trend-line for DonQi® duct, it can be observed that, $C_{T,D}$ decreases with increasing values of α. Conversely, for DonQi D5 duct, $C_{T,D}$ increases with increasing α. A local $C_{T,D}$ maximum at α = 17.5° appears for the DonQi D5 duct. The value of $C_{T,D}$ for DonQi D5 duct decreases for α beyond the local maximum.

The differences in the $C_{T,D}$ trend-lines for the two duct geometries can be explained by looking at the flow field. Contours of non-dimensional free-stream velocity $\frac{U_x}{U_\infty}$ for both duct geometries are reported in Figures 10 (a) to (h). Four yaw angles, i.e. α = 0°, 10°, 17.5° and 20°, are shown. The contours of DonQi® duct profile show that, with increasing values of α, the magnitude of velocity on the suction side of the duct decreases and the magnitude of velocity on the pressure side of the duct starts to increase significantly. This causes flow separation on the suction side of the duct. At α = 20°, the flow is completely separated from the duct surface and the duct is fully stalled. Inner duct wall flow separation is characterized by a strong reduction of duct wall shear stress which results in the reduction of $C_{T,D}$ with increasing α as shown in Figure 9. For the DonQi D5 duct, however, increased yaw returns higher velocity magnitude at the suction side of the duct up to α = 17.5°. This is due to the duct profile camber, which promotes flow acceleration on the suction side of the duct. The increased velocity magnitude on the suction side of the duct in this range is always accompanied by flow separation on the pressure side of the duct. As long as the flow separation is limited to the pressure side, the integral of duct thrust force coefficient $C_{T,D}$ in Figure 9 increases up to α = 17.5°. At α = 20°, the flow separation region traverses from the pressure side to the suction side of the duct indicating duct stalling characterized by the reduction of $C_{T,D}$ in Figure 9.

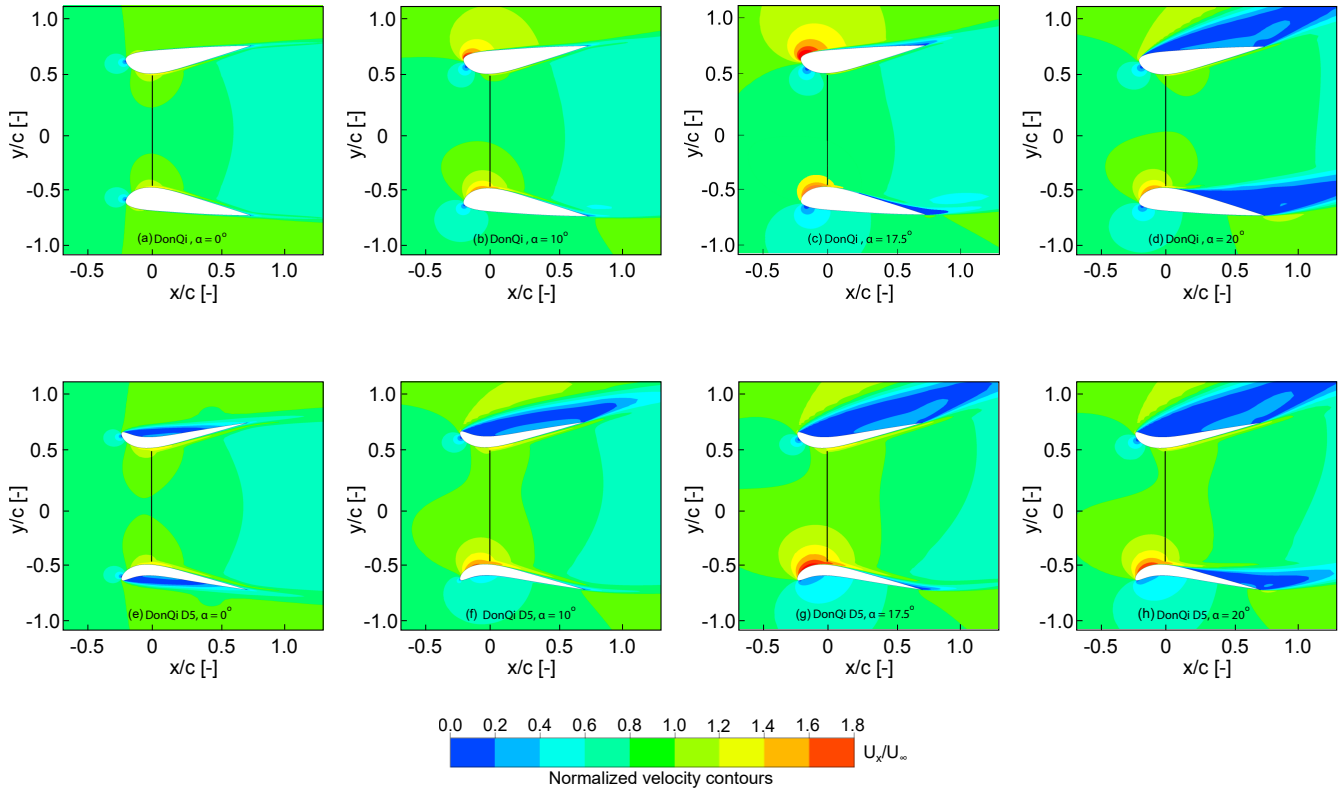

Figure 10. Velocity contours colored with streamwise normalized velocity. The results are depicted for DonQi duct-AD model (top) and DonQi D5 duct-AD model (bottom), both bearing a constant $C_{T,AD} = 0.7$.

5.3 Power Coefficient

Figure 11 represents the power coefficient C_P, for the two duct configurations, as a function of yaw angle α. For the sake of completeness, C_{P_o} for a bare AD is plotted alongside. The figure shows that, C_P is higher than C_{P_o} for all values of α. Comparing Figures 9 and 11, the C_P trends corresponds with the $C_{T,D}$ trends. The larger the $C_{T,D}$, the higher the C_P reached, and vice-versa. Similar to the $C_{T,D}$ trend for DonQi D5, maximum $C_P \approx 0.84$ is obtained for the DonQi D5 duct at $\alpha = 17.5°$; thereafter any further increase in α results in C_P drop. This also explains the experimental observations from Igra (1981), where a drop in the power coefficient for the duct-AD models with large duct expansion ratio was observed. For high duct expansion ratio, the likelihood of flow to separate from the inner walls of the duct increases (Abe and Ohya, 2004), thus lowering the $C_{T,D}$ and C_P values for a given duct-AD model.

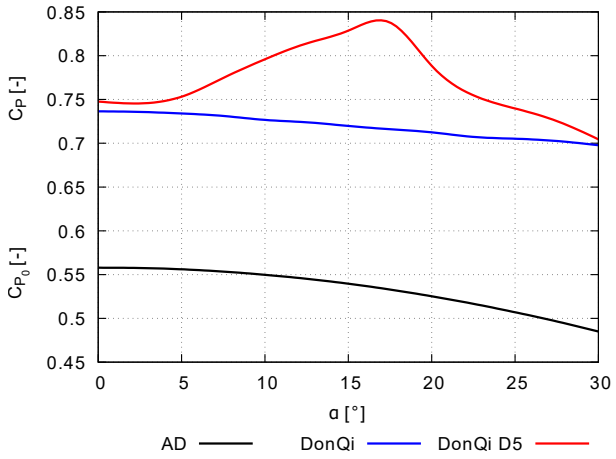

Figure 11. Effect of yawed inflow on the power coefficient.

6 Conclusions

In this work, the aerodynamic performance of DWTs in yawed flow is studied using a simplified duct-AD model. To this aim, two-dimensional numerical calculations using URANS simulations are shown. Based on the existing studies conducted by the authors, two duct geometries with different cross-section camber (named as DonQi® and DonQi D5) are chosen. To validate the numerical method, the comparison of numerical results with the experimental data are reported. Of the two duct geometries investigated, DonQi D5 duct configuration demonstrates a gain in the overall performance C_P up to at a yaw angle $\alpha = 17.5°$. On the contrary, C_P of DonQi® duct configuration drops for $\alpha > 0°$. The C_P gain for the DonQi D5 duct configuration with increasing α corresponds to the dimensionless duct thrust force coefficient $C_{T,D}$, which changes with duct geometry, AD (turbine) loading and inflow conditions. More precisely, inner duct wall flow separation reduces the $C_{T,D}$ and ultimately the C_P of the DWT model. The unsteady three-dimensional azimuthal effects, arising due to the turbine rotation within a duct, will have an impact on the aerodynamic performance of a DWT in yaw, and will be the subject of future work.

Appendix A: Nomenclature

c	Duct chord length [m]
C_P	Power coefficient for the duct-AD model [-]
C_{P_0}	Power coefficient for the bare AD [-]
$C_{T,AD}$	AD thrust coefficient [-]
$C_{T,D}$	Duct thrust coefficient [-]
C_T	Total thrust coefficient for the duct-AD model [-]
r	Augmentation factor [-]
S_{AD}	AD reference area [m^2]
S_e	Duct exit area [m^2]
T_{AD}	AD thrust force [N]
T_D	Duct thrust force [N]
T	Total thrust force for the duct-AD model [N]
U_{AD}	Normalized velocity at the AD plane [m/s]
U_{AD_0}	Normalized velocity for a bare AD [m/s]
U_∞	Free-stream velocity [m/s]
U_x	Stream-wise velocity component across the AD surface [m/s]
x	Variable value vector parallel to the free-stream direction [-]
y	Variable value vector normal to the free-stream direction [-]
α	Inflow yaw angle [$^\circ$]
ρ	Density of air [kg/m^3]
∞	Subscript representing quantity evaluated for free-stream condition
AD	Actuator disk
DWT	Ducted wind turbine
$HAWT$	Horizontal axis wind turbine
$LCOE$	Levelized cost of electricity

Author contributions. VVD compiled the literature review, setup the CFD simulations and wrote the bulk of the paper. DS performed the CFD simulations, post-processed the cases and contributed towards writing this paper. FA reviewed the paper and carried out modifications in different sections of this paper. GVB helped formulate the ideas in regular group discussions.

Competing interests. The authors declare that they have no conflict of interest.

Acknowledgements. Authors would like to acknowledge Prof. Ozer Igra for providing the experimental data that have contributed to the part of numerical validation reported in this paper. The research is supported by STW organization, grant number- 12728

References

Abe, K., Nishida, M., Sakurai, A., Ohya, Y., Kihara, H., Wada, E., and Sato, K.: Experimental and numerical investigations of flow fields behind a small wind turbine with a flanged diffuser, Journal of Wind Engineering and Industrial Aerodynamics, 93, 951–970, 2005.

Abe, K.-i. and Ohya, Y.: An investigation of flow fields around flanged diffusers using CFD, Journal of wind engineering and industrial aerodynamics, 92, 315–330, 2004.

Dighe, V. V., Avallone, F., Igra, O., and Bussel, G. v.: Multi-element ducts for ducted wind turbines: a numerical study, Wind Energy Science, 4, 439–449, 2019a.

Dighe, V. V., de Oliveira, G., Avallone, F., and van Bussel, G. J.: Characterization of aerodynamic performance of ducted wind turbines: A numerical study, Wind Energy, 2019b.

Dupont, E., Koppelaar, R., and Jeanmart, H.: Global available wind energy with physical and energy return on investment constraints, Applied Energy, 209, 322–338, 2018.

Fluent, A.: 14.0 User's Manual, ANSYS Inc., Canonsburg, PA, 2011.

Foreman, K. and Gilbert, B.: A Free Jet Wind Tunnel Investigation of DAWT Models, Grumman research and development Center Report to SERI, RE-668 (SERI/TR 01311-1), 1983.

Gielen, D., Boshell, F., Saygin, D., Bazilian, M. D., Wagner, N., and Gorini, R.: The role of renewable energy in the global energy transformation, Energy Strategy Reviews, 24, 38–50, 2019.

Gilbert, B. and Foreman, K.: Experiments with a diffuser-augmented model wind turbine, Journal of Energy Resources Technology, 105, 46–53, 1983.

Haans, W.: Wind turbine aerodynamics in yaw: unravelling the measured rotor wake, Ph.D. thesis, PhD thesis, TU Delft, 2003.

Igra, O.: Research and development for shrouded wind turbines, Energy Conversion and Management, 21, 13–48, 1981.

Khamlaj, T. and Rumpfkeil, M.: Theoretical Analysis of Shrouded Horizontal Axis Wind Turbines, Energies, 10, 38, 2017.

de Vries, O.: Fluid dynamic aspects of wind energy conversion, Tech. rep., Advisory Group for Aerospace Research and Development NEUILLY-SUR-SEINE (France), 1979.

Mikkelsen, R. and Sørensen, J.: Yaw analysis using a numerical actuator disc model, in: Proceedings of 14th IEA Symposium on the Aerodynamics of Wind Turbines, FFA, 14th IEA Symposium on the Aerodynamics of Wind Turbines ; Conference date: 04-12-2000 Through 05-12-2000, 2001.

Phillips, D., Richards, P., and Flay, R.: CFD modelling and the development of the diffuser augmented wind turbine, Wind and Structures, 5, 267–276, 2002.

Tang, J., Avallone, F., and van Bussel, G.: Experimental study of flow field of an aerofoil shaped diffuser with a porous screen simulating the rotor, International Journal of Computational Methods and Experimental Measurements, 4, 502–512, 2016.

Ten Hoopen, P.: An Experimental and Computational Investigation of a Diffuser Augmented Wind Turbine: with an application of vortex generators on the diffuser trailing edge, 2009.

Tongchitpakdee, C., Benjanirat, S., and Sankar, L.: Numerical simulation of the aerodynamics of horizontal axis wind turbines under yawed flow conditions, Journal of Solar Energy Engineering-Transactions of The ASME, 127, 464–474, 2005.

Toshimitsu, K., Nishikawa, K., Haruki, W., Oono, S., Takao, M., and Ohya, Y.: PIV measurements of flows around the wind turbines with a flanged-diffuser shroud, Journal of Thermal Science, 17, 375–380, 2008.

van Bussel, G.: The science of making more torque from wind: Diffuser experiments and theory revisited, Journal of Physics: Conference Series, 75, 120–10, 2007.

Versteeg, H. K. and Malalasekera, W.: An introduction to computational fluid dynamics: the finite volume method, Pearson education, 2007.

Werle, M. and Presz, W.: Ducted wind/water turbines and propellers revisited, Journal of Propulsion and Power, 24, 1146–1150, 2008.